IEEE Access
Multidisciplinary | Rapid Review | Open Access Journal

Received May 26, 2020, accepted June 19, 2020, date of publication June 29, 2020, date of current version July 13, 2020.

Digital Object Identifier 10.1109/ACCESS.2020.3005829

Statistical and Texture Descriptors of Symptomatic Plantar Fasciitis Using Ultrasound Shear Wave Elastography

HONGMEI ZHANG[1], (Member, IEEE), LEI XU[1,2], ZHIHUI LIU[1], SHUKUAN LU[1], (Associate Member, IEEE), JICHAO YIN[2], SIBO TIAN[3,4], XIAOFENG YANG[3,4], AND MINGXI WAN[1], (Member, IEEE)

[1]Key Laboratory of Biomedical Information Engineering of Ministry of Education, School of Life Science and Technology, Xi'an Jiaotong University, Xi'an 710049, China
[2]Department of Ultrasound, Xi'an Hospital of Traditional Chinese Medicine, Xi'an 710021, China
[3]Department of Radiation Oncology, Emory University, Atlanta, GA 30322, USA
[4]Winship Cancer Institute, Emory University, Atlanta, GA 30322, USA

Corresponding author: Mingxi Wan (mxwan@mail.xjtu.edu.cn)

This work was supported in part by the Social Development Fund of Shaanxi Province under Grant 2018SF-271, in part by the National Science Fund of China under Grant 61871316, in part by the National Key Scientific Instruments and Equipment Development Project under Grant 81827801.

ABSTRACT Plantar fasciitis (PFis) is a common cause of heel pain. This study aims to assess the plantar fascia (PF) quantitatively by using feature descriptors and seek valuable imaging biomarkers that can reliably diagnose PFis. A total of 63 participants underwent B-mode and longitudinal shear wave elastography (SWE) on unilateral plantar fasciae. To characterize the statistical and spatial texture features of the PF, ten statistical descriptors of the shear modulus in the standardized region of interest in PF and twenty texture descriptors in the SWE measurement window (in both horizontal and vertical directions) are proposed. Four statistical quantities (*mode, avg, med, qG*) and four texture descriptors (*autoc, sosvh, savgh svarh*) showed potential for diagnosing PFis, based on significant differences between the PFis and the healthy groups. Receiver operating characteristic (ROC) curve analysis revealed that the statistical descriptors have area under the curve (AUC) of approximately 0.9 (likelihood ratio > 6.798) and the texture descriptors have AUC of approximately 0.85 (likelihood ratio > 3.195). Combinations of statistical and texture descriptors can achieve higher AUCs$\sim$0.968. In addition, these descriptors were related to the clinical indices (body mass index and visual analogue scale) with Spearman's correlation coefficient of $r = -0.5 \sim -0.4 (p < 0.05)$. The proposed statistical and texture descriptors showed valuable potential if applied to clinical shear wave elastography for the diagnosis of PFis. This work lays the foundation of using ultrasound shear wave image features for describing symptomatic PFis.

INDEX TERMS Plantar fascia, shear modulus, statistical and texture descriptors, ultrasonography.

I. INTRODUCTION

The plantar fascia (PF) is mostly composed of type I collagen fibers forming bundles arranged in a proximal-distal direction, and the large fibrous bundles are embedded within a matrix of loose connective tissue containing type III collagen [1]. Healthy PF can bear greater loads by modifying its thickness and stiffness. Plantar fasciitis (PFis) is a musculoskeletal disorder primarily affecting the fascial enthesis, resulting from fiber microtears, collagen degeneration, chronic inflammation, and calcification caused by repetitive overstrain [2]. These microscopic changes within the PF may lead to reduction of elasticity. PFis can cause considerable heel pain and disability, seriously affecting activities of daily living [3].

PFis is primarily a clinical diagnosis, as determined by the orthopedist through an examination with tapping and touching combined with the visual analogue scale (VAS) score [4]. Plain radiography, magnetic resonance imaging (MRI) and ultrasound are common imaging modalities for evaluating

The associate editor coordinating the review of this manuscript and approving it for publication was Larbi Boubchir.

PFis [5]. MRI is sensitive for identifying PF disorders, but it is expensive and time-consuming. Ultrasound (US) imaging is an effective non-invasive method offering a better real-time assessment of PF echogenicity, thickness, ruptures, as well as intrafascial calcification, perifascial fluid collection, and fascial biconvexity [3].

Most US findings of plantar fasciitis include thickening of the plantar fascia, a diffuse hypoechoic area within the fascia band, and perifascial fluid [6]. Meta-analyses have revealed that the plantar fascia of those with chronic plantar heel pain (CPHP) were more likely to have a PF thickness of greater than 4.0 mm [7]. The combination of thickened PF and fat pad abnormalities on lateral plain radiography had a sensitivity of 85% and specificity of 95% for PFis [8]. Systematic reviews found that plantar fascia thickening and hypoechoic fascia are sonographic manifestations of PFis [3], [5], [9]–[11]. The hypoechogenic area in the plantar fascia usually represents a loss of normal fibrillar pattern where focal inflammation and diffuse tissue changes are present [3], [6].

However, not all patients with PFis exhibit these changes in tissue morphology and hypoechogenicity [6], [12], particularly for those with early-stage and preclinical disease [13]. Several reports have identified patients who had typical clinical manifestations of PFis but with normal plantar fascia morphology on B-mode sonography [10], [14]–[16]. Healthy PF can also display hypoechoic areas without thickening of the PF [10].

The development of PFis is thought to have a mechanical origin [2]. Early PFis is associated with the softening of the plantar fascia due to loss of fibrillar pattern. Sonoelastography or strain imaging, is a promising method to characterize the early changes in PFis, where a significant amount of force is required to externally compress the heel pad to induce a deformation for measuring the PF stiffness. Several studies reported sonoelastography results of PFis showing a softening of the PF on the affected side, whereas conventional ultrasound reported normal PF echogenicity and thickness. Others reported that the plantar fascia was softer in patients with PFis compared to healthy controls [14]–[18].

However, sonoelastography is a user-dependent method. Due to the highly nonlinear deformation behavior of the heel pad, the measured stiffness is dependent on the magnitude of the applied force and loading rate. Consequently, studies using different instruments and loading conditions yield inconsistent results, which results in uncertainty of the diagnosis.

Ultrasound shear wave elastography (SWE) is a novel non-invasive technology to characterize the mechanical property of tissues. When compared to compression sonoelastography, SWE is more objective, quantitative, and reproducible [13]. In SWE, the acoustic radiation force is generated by the ultrasound probe to perturb the tissue in the focal area, inducing shear waves that propagate transversely within the tissue. The shear wave propagation speed v is captured by the ultrasound transducer at an ultrafast frame rate and the velocity can be tracked by a correlation algorithm. The tissue shear modulus can be estimated by $G = \rho v^2$ where ρ is the density of the tissue [19]. The elastic image of the tissue can be formed by queue emission and successive tracking of the shear waves at different locations. As SWE exhibits excellent retest reliability, it can quantitatively characterize soft tissue stiffness. Recently, SWE has been used to map the elastic distribution of the heel pad and PF near the calcaneus [11], [19]–[24].

Current elastography methods (either strain or SWE imaging) use color channel image information to assess the PF, where stiffness has been quantized into several color grades [14], [15], [17], [18]. However, these methods depend on the musculoskeletal radiologist's visual diagnosis and are not sufficient to characterize PFis. Quantized color histogram analyses of sonoelastography showed that 72.7% of fasciae were of intermediate elasticity and no significant association with fasciitis [17]. Another study reported that the PF softens with age in subjects with PFis [18].

Due to the complex stiffness distribution, characterizing PF is also highly site-dependent [20], [21], [24], [25]. The proximal sites of PF around the calcaneal attachment were reported to be significantly thicker and stiffer than the middle and distal sites [21]. The analysis of PF was conducted at continuous locations which were trivial [20]. PF elasticity was also evaluated at different locations of the calcaneus and averaged in a relatively small standardized region [24]. Quantitative indices such as the maximum, minimum, and median or spatially averaged elastic modulus value over the whole PF have been proposed, but they are not sufficient to describe the features of the PF [17], [24]. Therefore, valuable feature descriptors to quantitatively characterize the complex site-dependent elastic distribution and to extract echovariation texture features by SWE imaging are needed.

Statistical and texture features are useful descriptors for characterizing complex biological tissue [26]–[29]. Widely used statistical quantities include maximum, minimum, median or mean values of the data set, but the statistical distribution features are rarely reported. In our previous work, statistical descriptors of the peak and distribution moments (coefficient of variation, skewness and kurtosis) of Von Mises strain images were proposed and used to identify vulnerable carotid plaques [26]. Others used statistical descriptors, such as quantiles and distribution moments for the identification of cervical cancer in MRI images [27]. Textures are important features that depict image echovariance. Using texture features for analyzing PF has not been previously reported. Texture features has been used for identifying other diseased tissues. For example, texture extracted from strain rate images were proposed for vulnerable plaque identification [28]. Recent studies using machine learning (ML) approach is another promising branch in the diagnosis of early disease [30], [31]. Textures can also be combined with machine learning method to select valuable features. Identification of liver tumors from ultrasonography was proposed based on texture features and fuzzy support vector

machine (SVM) method [29]. However, extensive training is needed for ML approach that is time-consuming.

The aim of this study is to seek clinically applicable biomarkers for the diagnosis of PFis. The contribution of this work is as follows. SWE images of PF, which can depict early PF disease with good reproducibility, were analyzed. Considering the heterogeneous distribution of PF, ten statistical descriptors including the distribution moments were proposed. As normal PF and PFis showed different echovariance in the periphery of the calcaneus in SWE image, seeking valuable texture descriptors to depict the echovariation feature of PF were investigated. Furthermore, to increase the clinical applicability, the descriptors were measured in specific region of interest for retest reliability, where statistical quantities of shear modulus were measured in a standardized region of interest (SROI) in PF and the texture descriptors were extracted in the SWE measurement window. Additionally, proper descriptors are identified, and the feasibility of these descriptors for diagnosing PFis was confirmed by statistical analysis and cross validation.

II. METHODS

A. STUDY PROTOCOL

The study was approved by the ethics committee of the Institutional Review Board/The Ethics Committee of Xi'an Hospital of Traditional Chinese Medicine (No. XAZYYLS2017-26). A written informed consent was given by all participants. Patients met the following criteria: 1) pain duration longer than 3 months; 2) have not received steroid injections, have not undergone shock wave therapy or heel surgery; 3) no calcaneal spur confirmed by X-ray; 4) unilateral foot pain. To minimize the impact of selection bias, healthy adults with similar body conditions were recruited as volunteers to participate in the study. Patients were diagnosed with PFis by orthopedic surgeons according to the clinical practice guidelines of heel pain-plantar fasciitis (Revision 2014) [4]. Ultrasonography was performed by clinicians specializing in musculoskeletal sonographic imaging following a standardized physical examination. The real-time examination included B-mode scanning and shear wave elastography (SWE) using a commercial ultrasound system (Mindray Resona 7) equipped with a linear array transducer L14-5WU (9∼14MHz). Patients were positioned prone with their feet hanging over the edge of the examination table during acquisition. A longitudinal view of the plantar fascia was acquired from the anterior edge of the inferior calcaneal border vertically to the inferior border of the plantar fascia. The maximal thickening of the plantar fascia was measured from the B-mode ultrasound. Meanwhile, real-time visualization of a color quantitative elasticity map (representing the shear modulus of the soft tissue) superimposed on a B-mode image was acquired using SWE imaging.

In total 63 participants were included in the study (25 healthy participants and 38 symptomatic unilateral PFis.). General clinical characteristics of the study populations are summarized in Table 1. There were no significant differences in age, height and gender between the healthy volunteers and the PFis groups. The body mass index (BMI) of the PFis group (25.21±2.41 kg/m^2) was significantly higher than that of the Healthy group (22.88±3.33 kg/m^2). The PF thickness of the PFis group (3.51±1.00 mm) was also significantly higher than that of the Healthy group (2.46±0.58 mm).

B. SHEAR WAVE ELASTOGRAPHY (SWE) ANALYSIS

Shear wave elastography was conducted on the calcaneal attachments which are the most frequently affected PFis site. The SROI in the PF was outlined individually around the calcaneus attachment, using a consistent protocol for all participants. This standardized elliptic region was selected near the calcaneus where the left end of the ellipse started at the disappearance of the foot margin. The long axis was set along the PF centerline, and the short axis was close to the PF thickness but smaller than it to avoid the effect of the fat pad. Ten statistical quantities were calculated to characterize the distribution of the shear modulus within the SROI. As previously reported, PF thickening, abnormalities in the fat pad deep below the PF and bone cortical changes in the calcaneus were radiographic findings of PFis [2], [8], [21]. Therefore, the SWE measurement window was selected below the heel skin and included the fat pad, the plantar fascia and the calcaneus. The size of the SWE-measurement rectangle window was approximately 5.6 cm^2. Based on the selected rectangle region, GLCM was calculated, from which twenty texture features were extracted to characterize the echovariation of the shear modulus image.

1) STATISTICAL DISTRIBUTION FEATURES

Statistical distribution features of the shear modulus within the SROI were quantified by ten statistical descriptors. G denotes shear modulus, and $p(G)$ is the normalized histogram of the shear modulus G. $G_{a\%}$ denotes the a% quantile of G. μ is the mean value of G and S the sample standard deviation. $E[\mathrm{x}]$ indicates the mathematical expectation of x. The distribution of G can be characterized by the quantities including the mode (*mode*), mean value (*avg*), median value (*med*), peak value (*Mx*), 25% quartile (*qG*), range (*R*), quartile deviation (*Rq*), coefficient of variation (*Vs*), skewness (*SK*) and kurtosis (*K*) [32]. A detailed definition of the descriptors is provided in Table 2.

2) TEXTURE DESCRIPTORS

Texture is an important feature descriptor. The co-occurrence probabilities provide a second-order method for generating texture features [33]. They represent the conditional joint probabilities of all pair wise combinations of gray levels in the spatial window of interest given two parameters: interpixel distance (d) and orientation (θ).

Let (x_1, y_1), (x_2, y_2) denote the coordinates of the pixel pair in the gray-level image I, with gray levels of $I(x_1, y_1) = i$, $I(x_2, y_2) = j$ respectively. $P(i, j)$ denotes the GLCM of the

TABLE 1. General clinical characteristics of the study population.

Variable	Healthy (n=25)		Plantar fasciitis(n=38)		p-value*
	Mean(SD)	95%CI	Mean(SD)	95%CI	
Age (year)	40.84 (14.70)	34.77-46.91	43.74 (8.42)	40.97-46.50	0.188
Height (m)	1.69 (0.06)	1.66-1.72	1.67 (0.08)	1.64-1.70	0.343
Weight (kg)	65.6 (12.31)	60.52-70.68	70.53 (10.04)	67.23-73.83	0.087
Body mass index (kg/m^2)	22.88 (3.33)	21.50-24.25	25.21 (2.41)	24.42-26.00	0.002
Thickness (mm)	2.46 (0.58)	2.22-2.70	3.51 (1.00)	3.18-3.84	p<0.001
Gender (male)	16 (25)		18 (38)		0.195

*ANOVA for independent samples or Mann-Whitney test where appropriate
SD = standard deviation; CI = 95% confidence interval;

TABLE 2. Ten statistical descriptors for characteristic of the distribution feature.

Variable	Formula	Annotation
mode	$\arg\max_G(p(G))$	Mode of G, the value occurring most frequently in a data set
avg	$\frac{1}{N}\sum G$	Mean value of G
med	$G_{50\%}$	Median value of G
Mx	$max(G)$	Peak value of G
qG	$G_{25\%}$	25% quartile of G
R	*MxG-MnG*	Range
Rq	$G_{75\%}$-$G_{25\%}$	Deviation of quartile
Vs	S/μ	Coefficient of variation
SK	$\frac{E[(X-\mu)^3]}{([E[(X-\mu)^2]])^{3/2}}$	Skewness
K	$\frac{E[(X-\mu)^4]}{([E[(X-\mu)^2]])^2}$	Kurtosis

relative frequencies with which two neighboring resolution cells separated by distance d occur on the image, one with gray level i and the other with gray level j. The normalized GLCM of the gray-level image is defined by (1), as shown at the bottom of the next page, where $\#P$ is the total number of possible pixel pairs.

Barber and LeDrew demonstrated that $d = 1$ produced a significantly superior classification when compared with others [34]. In this study, the distance was chosen as $d = 1$. The GLCMs in horizontal ($\theta = 0$) and vertical ($\theta = 90°$) directions were calculated. The quantized number of gray levels G_n was set to be 256.

Twenty texture descriptors were derived from the GLCM and used for texture descriptors in shear wave images. In this study, four texture descriptors including autocorrelation (*autoc*), sum of squares (*sosvh*), sum average (*savgh*), and sum variance (*svarh*) were chosen as feature descriptors based on GLCM as shown in Table 3. Other texture descriptors are provided in Appendix.

C. STATISTICAL ANALYSIS

Statistical analysis was conducted by SPSS Version 18.0 (IBM, Armonk, NY, USA) and MATLAB (The MathWorks, Natick, MA, USA). All descriptive data was expressed as either the mean with standard deviation or frequency (%). Tests of normality and homogeneity of variances between the two distributions were assessed by Shapiro–Wilks and Levene's tests, respectively. Comparisons of parameters between the two groups were performed by one-way ANOVA or Mann-Whitney test where appropriate. Two-tailed post hoc tests were performed. Values of $p < 0.05$ were considered statistically significant. A receiver operating characteristic (ROC) curve analysis on the descriptors for diagnosing PFis was conducted. The area under curve (AUC), the optimal threshold for test quantities and the likelihood ratio, as defined by *sensitivity/(1-specificity),* were calculated. The correlation between two continuous variables was described by Pearson coefficient for normally distributed data. The correlation between two non-normally distributed continuous variables or qualitative data was measured using Spearman's correlation coefficient where appropriate. The Co factors ROC analysis was conducted by support vector machine (SVM) method [35].

III. RESULTS

A. SHEAR WAVE IMAGING OF PLANTAR FASCIA

Fig.1 displays four representative shear modulus overlapping B-mode images, together with the histogram of the shear modulus in the SROI and the horizontal GLCM in the rectangular measurement window. Table 4 shows the values of the descriptors for four representative subjects. The four statistical descriptors of the shear modulus (*mode, avg, med, qG*) were much higher in healthy PF than those in PFis, due to healthy PF being capable of bearing greater loads for its higher elasticity. From the SWE images, healthy PF showed a layered fibrillar pattern that contributes to its elasticity. The histogram of the healthy PF revealed a broad elastic distribution with the mode of around 40kPa, which corresponds to the layered fibrillar structures. In contrast, PFis was considered with microscopic tears within the fascia, leading to reduction of its elasticity. The SWE image showed that PFis had relative homogeneous focal soft areas with loss of fibrillar patterns leading to inflammatory exudates that decreased elasticity [6]. Therefore, the elastic

TABLE 3. Four texture descriptors for characteristic of the image feature.

Variable	Formula	Annotation
autoc	$\sum_i \sum_j (ij)p(i,j)$	Autocorrelation measures the interpixel correlation
sosvh	$\sum_i \sum_j (i-\mu)^2 p(i,j)$	Sum of squares is also the variance
savgh	$\sum_{i=2}^{2G_n} i p_{x+y}(i)$	Sum average
svarh	$\sum_{i=2}^{2G_n} \left(i - \left[- \sum_{i=2}^{2G_n} p_{x+y}(i) log \left\{ p_{x+y}(i) \right\} \right] \right)^2 p_{x+y}(i)$	Sum variance

Where $p \quad (k) = \sum^{G_n} \sum^{G_n} p(i\ j) | i + j = k \ \ k = 2\ 3 \quad 2G$

TABLE 4. Statistical and texture descriptors for the four representative subjects.

Group	Statistical descriptors (kPa)				Texture descriptors				
	mode	*avg*	*med*	*qG*	Orientation	*autoc*	*sosvh*	*savgh*	*svarh*
Healthy1	38.21	36.66	37.32	34.05	Horizontal	5614.19	5650.24	133.93	21095.05
					Vertical	5634.04	5636.65	133.91	21126.14
Healthy2	43.38	41.39	43.00	35.13	Horizontal	5931.11	5971.06	134.93	22355.51
					Vertical	5956.49	5959.07	134.90	22391.68
PFis1	10.48	11.90	11.50	10.70	Horizontal	2593.18	2621.50	95.73	9512.93
					Vertical	2618.02	2622.35	95.89	9582.35
PFis2	9.94	13.20	11.99	9.59	Horizontal	4765.61	4796.59	123.65	17836.10
					Vertical	4788.32	4796.24	123.66	17876.28

distribution for PFis was narrow and the mode was approximately 10kPa. GLCM is a joint probability density for interpixel with specific structure and spatial relation, from which the texture descriptors are defined. The third column in Fig.1 provides the horizontal GLCM, representing the co-occurrence frequency of the interpixel with $d = 1$ in the horizontal direction. The GLCMs for healthy PF were broader with longer tails, whereas the GLCMs for PFis were more compact, indicating that a healthy PF was more heterogeneous due to its layer fibrillar pattern. The four texture descriptors (*autoc, sosvh, savgh, svarh*) in healthy PF were much higher than those in PFis, as healthy PF had higher elasticity and heterogeneity.

B. COMPARISION OF DESCRIPTORS IN THE HEALTHY AND PLANTAR FASCIITIS GROUPS

1) STATISTICAL DESCRIPTORS IN THE HEALTHY AND PLANTAR FASCIITIS GROUPS

The comparisons of the statistical descriptors are provided in Fig. 2. The statistical quantities of the shear modulus (*mode, avg, med, qG, Mx, R, Rq*) in healthy PF were significantly higher than those in PFis group. The skewness in the PFis group was significantly higher than that of the Healthy group. There were no significant differences in terms of *Vs* ($p = 0.978$) and *K* ($p = 0.053$) between the Healthy and PFis groups. The detailed statistical results of statistical descriptors are provided in Table S1.

2) TEXTURE DESCRIPTORS IN THE HEALTHY AND PLANTAR FASCIITIS GROUPS

The comparison of the texture descriptors are provided in Fig. 3. All four descriptors (*autoc, sosvh, savgh, and svarh*) were significantly higher in the Healthy group than those with PFis, in both the horizontal and the vertical directions. Also, the texture descriptors from the horizontal GLCM were in strong agreement with their vertical counterparts. The detailed results are provided in Table S2-1 and Table S2-2 for horizontal and vertical texture descriptors respectively.

C. CORRELATION ANALYSIS

1) CORRELATION WITH CLINICICAL INDICES

PF thickness has been reported to be an early sign of PFis [3], [5], [9]–[11]. Systematic reviews and meta-analyses of various clinical and imaging risk factors have reported higher BMI in those with PFis being the only significant clinical association [36]. Similar reports have found that increased BMI was linked to decreased stiffness and increased thickness of the PF [22]. The pain of PFis can be assessed by VAS [15]. Therefore, the correlation between the proposed

$$p(i,j) = \#\{(x_1,y_1),(x_2,y_2) \mid |x_1 - x_2| = dcos\theta, |y_1 - y_2| = dsin\theta, I(x_1,y_1) = i, I(x_2,y_2) = j\} / \#P \quad (1)$$

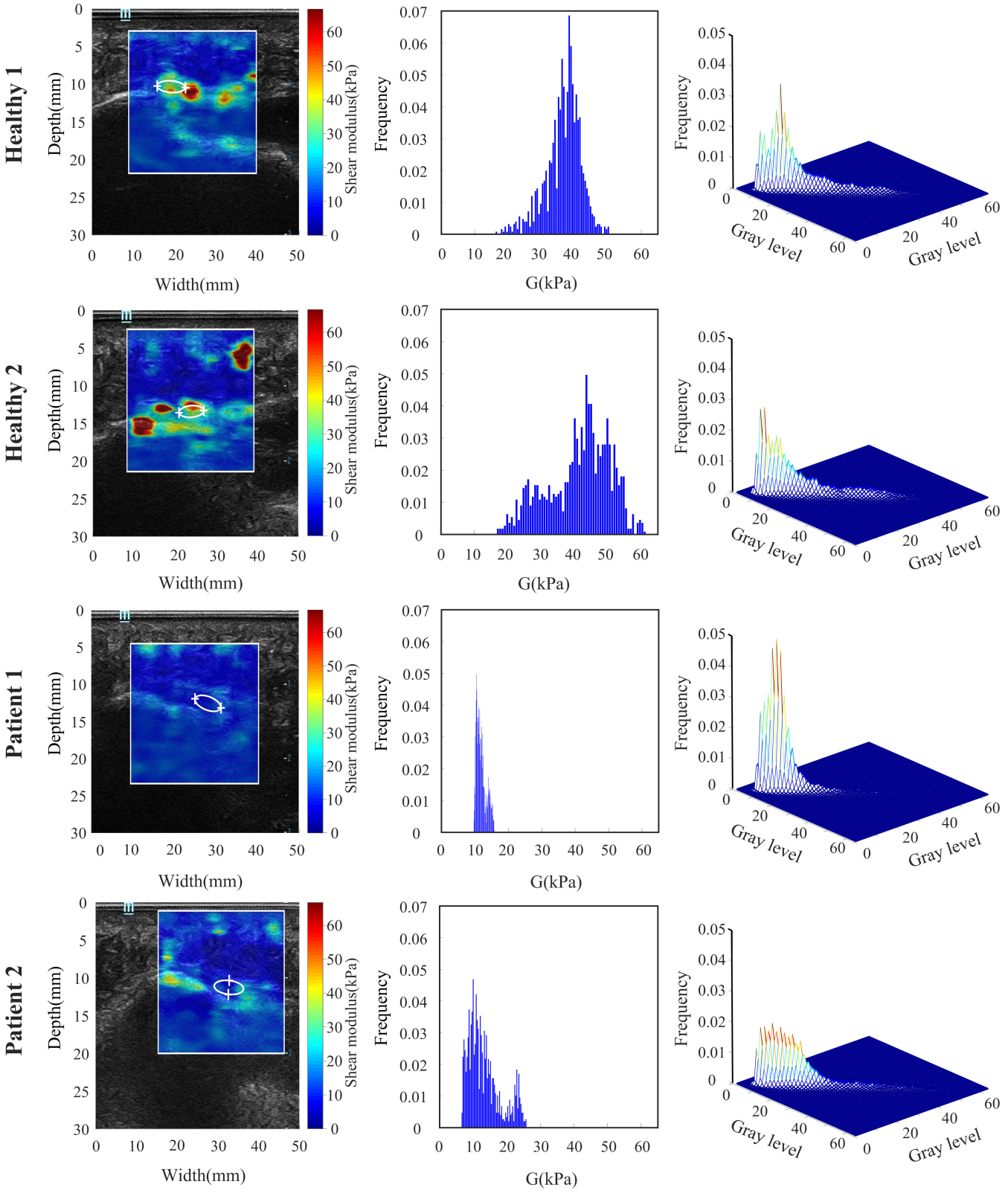

FIGURE 1. Representative shear wave elastography analysis for healthy plantar fascia and PFis. The first column shows the shear modulus overlapping B-mode image. The white rectangle indicates the SWE measurement window. The second column shows the histogram of the shear modulus in the SROI (as indicated by the white ellipse). The histogram was quantized into 64 gray levels for visualization purpose. The third column shows the GLCM in the horizontal direction.

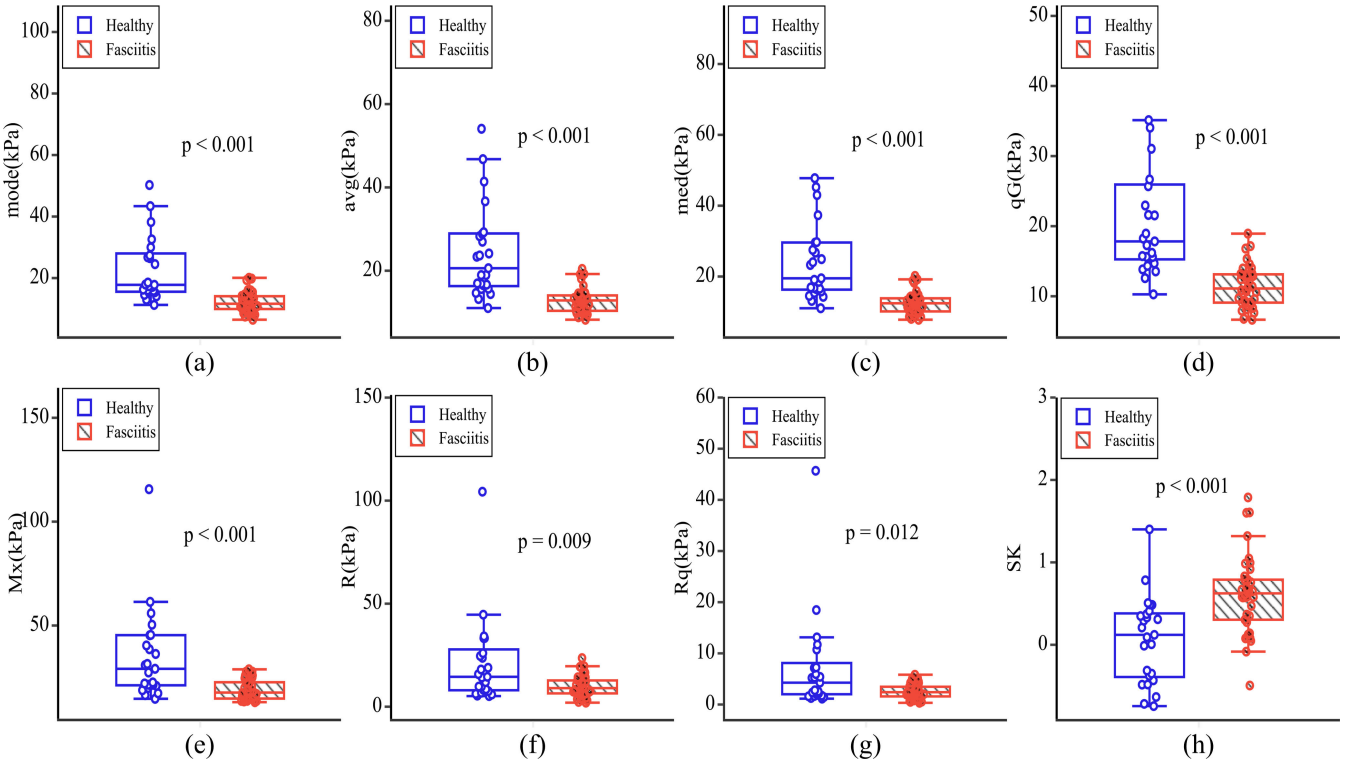

FIGURE 2. Comparison of the statistical descriptors (mode, avg, med, qG, Mx, R, Rq, SK) between the Healthy and the PFis groups. Blue dots are the statistical descriptors for the healthy PF and red dots indicate the PFis subjects.

descriptors (statistical and texture descriptors) and these potential clinical indices was analyzed.

As shown in Table 5, four statistical descriptors negatively correlated with the BMI ($r = -0.510$~-0.480, $p < 0.001$). There were also negative correlations between the BMI and the texture descriptors ($r \sim -0.38$, $p = 0.002$).

There was a negative correlation between the thickness and mode($r = -0.416$, $p = 0.001$). The Spearman correlation between the thickness and other descriptors was $r = -0.289$~ -0.249 ($p < 0.049$).

There was a negative correlation between VAS and statistical descriptors ($r = -0.563$~ -0.557, $p < 0.001$). A negative correlation was also observed between the VAS and the texture descriptors ($r = -0.432$~ -0.423, $p \leq 0.001$) in both horizontal and vertical directions.

A negative correlation was also present between weight and the statistical descriptors ($r = -0.350$~ -0.344, $p < 0.006$), whereas there was no correlation between age or height and the proposed descriptors ($p > 0.05$).

2) INDEPENDENCY ANALYSIS ON PARAMETERS

The independency of all other parameters was tested, and the detailed results are provided in Table S3. The results showed that the four statistical descriptors were highly correlated ($r \geq 0.960$, $p < 0.001$), and the four texture descriptors also correlated strongly ($r \geq 0.982$, $p < 0.001$). The correlation between the statistical and the texture descriptors ranged from $r = 0.603$ to 0.631 ($p < 0.001$). For clinical indices, BMI correlated with the thickness ($r = 0.513$, $p < 0.001$). Weight correlated with the BMI ($r = 0.828$, $p < 0.001$), with thickness ($r = 0.372$, $p = 0.003$), and with height ($r = 0.667$, $p < 0.001$).

D. ROC ANALYSIS

1) SINGLE FACTOR ROC ANALYSIS

ROC analysis of the proposed descriptors was conducted and compared with those of clinical indices. The detailed AUC values, thresholds and likelihoods are provided in Table S4.

ROC curves of statistical quantities for which the AUC was above 0.85 are shown in Fig. 4a. The 25% quartile (*qG*) showed the highest potential for diagnosing PFis, which has AUC = 0.917±0.036 ($p < 0.001$) with a high likelihood ratio of 10.197. Other quantities, such as *mode* (AUC = 0.899±0.038, $p < 0.001$), *avg* (AUC = 0.907±0.038, $p < 0.001$) and *med* (AUC = 0.907±0.038, $p < 0.001$) were also capable of indicating PFis (likelihood ratios ≥ 6.798).

As shown in Fig.4b, the texture descriptors from the horizontal GLCM such as *autoc* (AUC = 0.845±0.054, $p < 0.001$), *sosvh* (AUC = 0.847±0.053, $p < 0.001$), *savgh* (AUC = 0.848±0.050, $p < 0.001$) and *svarh* (AUC = 0.845±0.054, $p < 0.001$) were capable of indicating PFis (likelihood ratios ≥ 3.195). In Fig. 4c, texture descriptors from the vertical GLCM such as *autoc* (AUC = 0.846±0.054, $p < 0.001$), *sosvh* (AUC = 0.847±0.053, $p < 0.001$), *savgh*

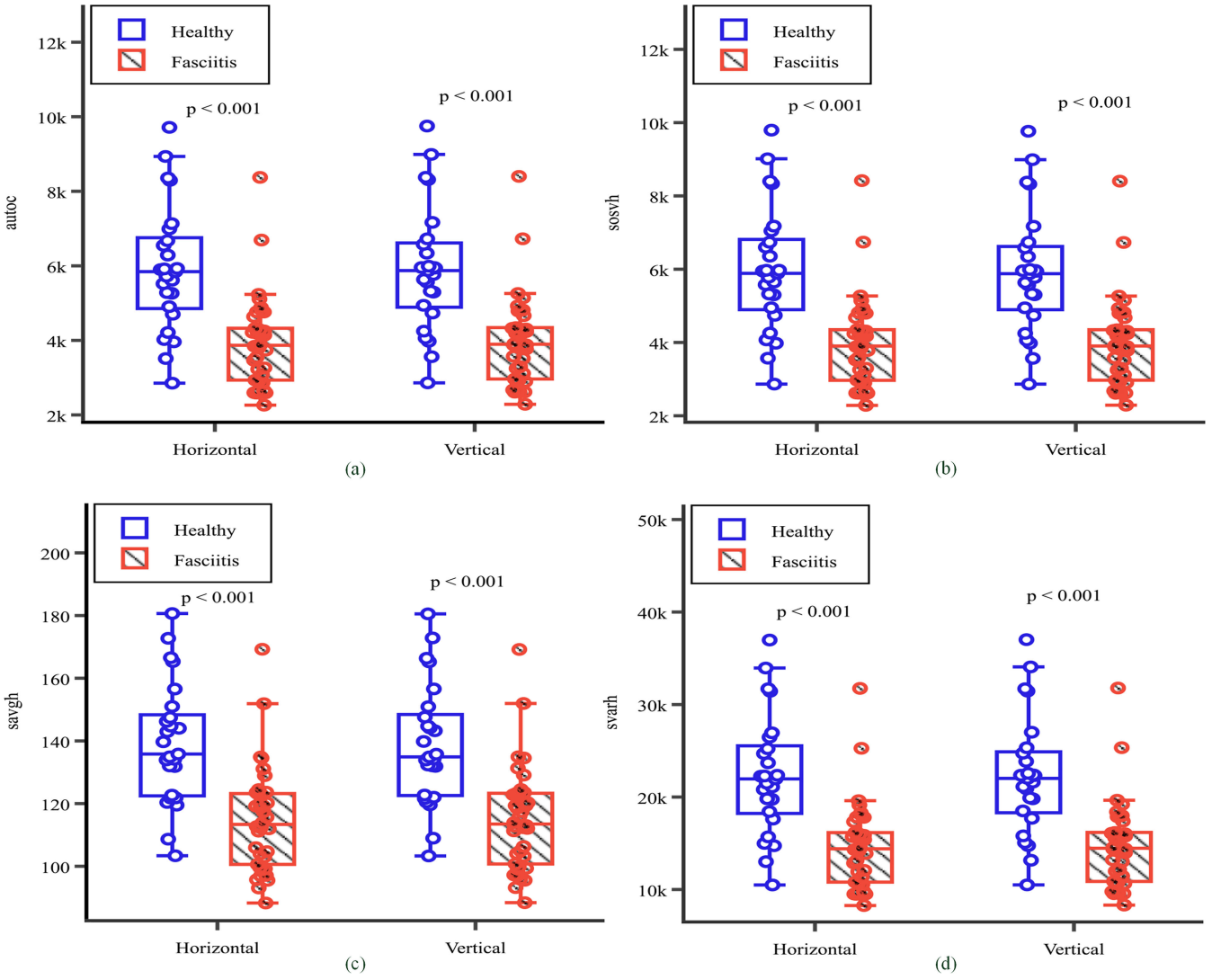

FIGURE 3. Comparison of texture descriptors (autoc, sosvh, savgh, svarh) between the Healthy and the PFis groups. Blue dots are texture descriptors for the healthy PF and red dots indicate the PFis subjects.

TABLE 5. Correlation of the proposed descriptors and clinical indices.

Spearman Correlation	variable	Thickness(mm)	BMI(kg/m²)	VAS	age(year)	height(m)	weight(kg)
Statistical descriptors	*mode(kPa)*	-0.416(p=0.001)	-0.510(p<0.001)	-0.561(p<0.001)	-0.120(0.349)	0.030(0.813)	-0.350(0.005)
	avg(kPa)	-0.252(0.046)	-0.480(p<0.001)	-0.557(p<0.001)	-0.146(0.255)	0.011(0.929)	-0.346(0.005)
	med(kPa)	-0.229(0.071)	-0.486(p<0.001)	-0.563(p<0.001)	-0.143(0.264)	0.022(0.864)	-0.344(0.006)
	qG(kPa)	-0.289(0.022)	-0.485(p<0.001)	-0.563(p<0.001)	-0.126(0.326)	0.018(0.864)	-0.350(0.005)
Horizontal texture descriptors	*autoc*	-0.267(0.034)	-0.379(0.002)	-0.428(0.001)	-0.120(0.349)	0.062(0.631)	-0.201(0.115)
	sosvh	-0.267(0.034)	-0.377(0.002)	-0.430(p<0.001)	-0.120(0.350)	0.067(0.600)	-0.194(0.127)
	savgh	-0.249(0.049)	-0.331(0.008)	-0.432(p<0.001)	-0.082(0.522)	0.086(0.501)	-0.167(0.192)
	svarh	-0.268(0.034)	-0.380(0.002)	-0.428(0.001)	-0.124(0.334)	0.067(0.601)	-0.197(0.122)
Vertical texture descriptors	*autoc*	-0.270(0.032)	-0.378(0.002)	-0.429(0.001)	-0.120(0.348)	0.068(0.598)	-0.195(0.125)
	sosvh	-0.270(0.032)	-0.378(0.002)	-0.429(p<0.001)	-0.116(0.363)	0.067(0.600)	-0.195(0.125)
	savgh	-0.251(0.047)	-0.328(0.009)	-0.423(0.001)	-0.079(0.540)	0.082(0.522)	-0.166(0.192)
	svarh	-0.271(0.032)	-0.379(0.002)	-0.431(p<0.001)	-0.122(0.340)	0.069(0.589)	-0.193(0.129)

(AUC = 0.844±0.051, $p < 0.001$) and *svarh* (AUC = 0.846±0.054, $p < 0.001$) were also capable of indicating PFis (likelihood ratios ≥ 3.195). The texture descriptors from the horizontal GLCM agreed with those from the vertical GLCM.

As shown in Fig. 4d, using clinical indices as test statistics, AUC = 0.728±0.069 ($p = 0.002$) for BMI with likelihood ratio of 2.820 and AUC = 0.778±0.059 ($p < 0.001$) for thickness with likelihood ratio of 2.632. When using other indices

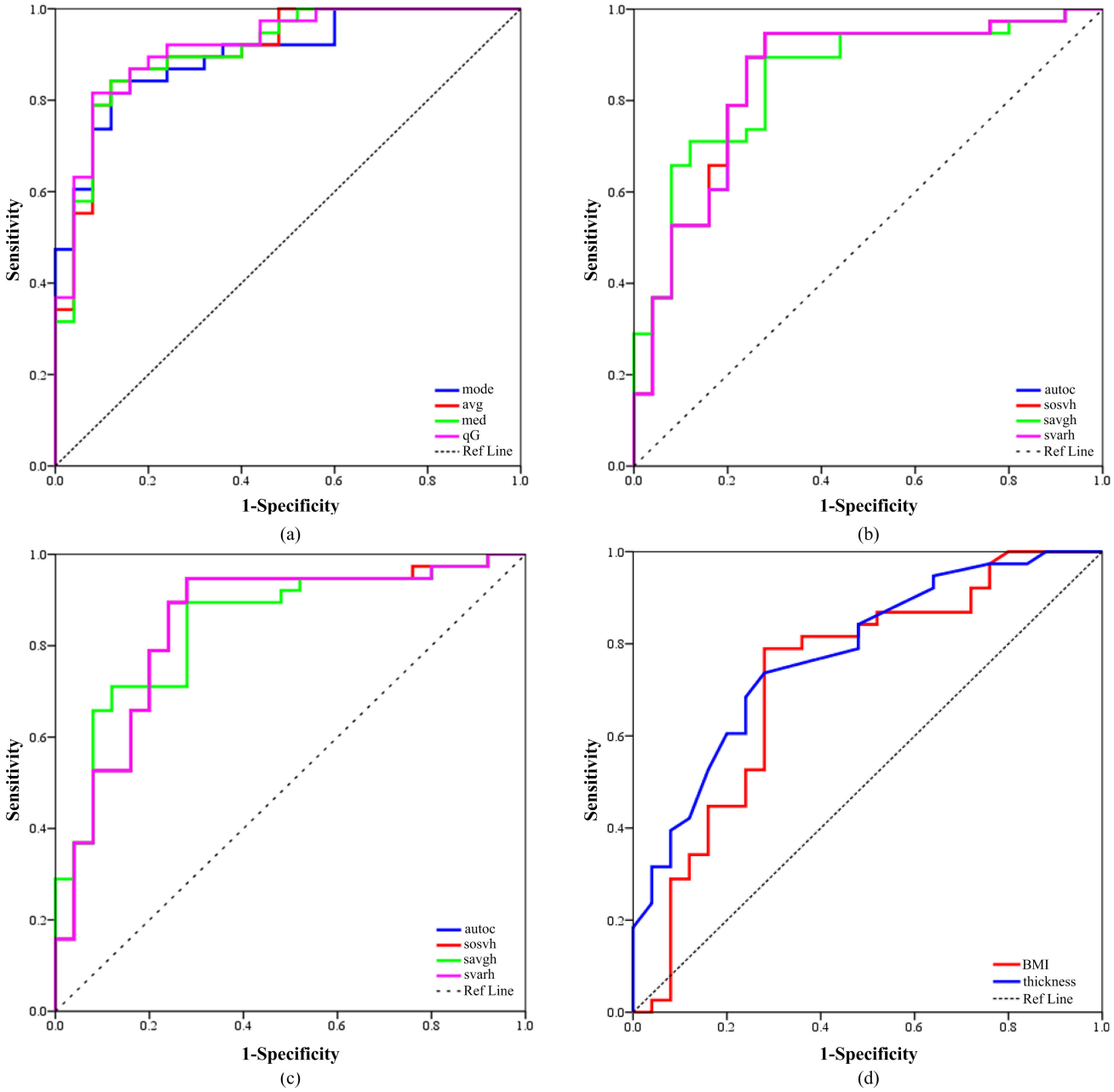

FIGURE 4. ROC curves of statistical descriptors (a), texture descriptors from the horizontal GLCM (b) and from the vertical GLCM (c), and clinical indices (d).

such as gender, age, height, and weight as test statistics, AUCs were not statistically significant ($p > 0.05$).

The ROC analysis revealed that the four statistical descriptors (*mode, avg, med, qG*) had high AUCs (∼0.9) with sensitivity (≥0.816), specificity (≥0.88) and high likelihood ratio (≥6.798). Using the four descriptors as test quantities to diagnose PFis, the AUCs were clustered at 0.85±0.05 ($p < 0.001$) with sensitivity ≥ 0.895, specificity = 0.72, and likelihood ratios ≥3.195. Using clinical indices as test quantities, AUC ≤ 0.778, with sensitivity ≤0.789, specificity = 0.72 and likelihood ratio ≤ 2.820.

The results confirm that the proposed statistical and texture descriptors are potential biomarkers for the diagnosis of PFis, which have better diagnostic performance compared to clinical indices (BMI and thickness).

2) CO FACTORS ROC ANALYSIS

The co factors ROC analysis was conducted by SVM using a 5-fold cross-validation scheme. As provided in Table S5, the co factors only including the statistical descriptors dominated with higher AUCs of 0.93∼0.951, and only the texture descriptors dominated with AUCs of 0.861∼0.868, whereas the features only with the clinical indices presented with AUCs of 0.72∼0.83.

The combination of statistical and texture descriptors achieved higher AUCs of 0.868∼0.968. By combining the

statistical descriptors and the clinical indices, the AUCs were 0.787∼0.967, and by combining the texture descriptors and the clinical indices, the AUCs were 0.852∼0.926. When combining the three kinds of features (statistical descriptors, texture descriptors, and clinical indices), the AUCs were 0.862∼0.964.

The co factors ROC analysis revealed that by combining statistical descriptors or texture descriptor into the feature vectors, AUCs were further improved. The proposed statistical descriptors and texture descriptors are important features and could achieve a high diagnostic accuracy.

IV. DISCUSSION

Multiple statistical descriptors (*mode, avg, med, qG*) in the SROI and texture descriptors (*autoc, sosvh, savgh*, *svarh*) from the SWE measurement window were identified that were notable SWE predictors for PFis. There were significant differences in these descriptors between Healthy and PFis groups. These descriptors had high AUCs (∼0.9 for statistical descriptors and ∼0.85 for texture descriptors), and correlated with clinical parameters.

A. DIFFERENCE ANALYSIS ON THE HEALTHY AND PLANTAR FASCIITIS GROUPS

The shear modulus distribution features such as *mode, avg, med, Mx*, and *qG* in the healthy PF were significantly higher than those in the PFis group. The results support the findings of PF softening in subjects presenting with characteristic symptoms of PFis [18]. The range *R* and quartile deviation *Rq* in the healthy PF were also significantly higher than in the PFis group, indicating that the PFis group showed much more homogeneity than the Healthy group. The results confirm results from previous study where hypoechogenicity was another sign of PFis in B mode ultrasound images [3], which corresponds to the softer tissue (with lower elasticity) in the elastography.

The proposed texture descriptors showed significant differences between the Healthy and PFis groups, in both the horizontal and vertical directions. The texture descriptors from the horizontal and the vertical GLCM were in strong agreement. The texture descriptors can depict the PF well since the shear modulus of healthy tissue and PFis had significant texture differences in terms of the fabric structure. It can be seen from the shear modulus elastography in Fig.1 that the healthy tissues showed clear fibrillar structure whereas the PFis tissues showed softer homogenous regions due to the loss of fibrillar patterns. The results of this study agreed with previous work in that echotexture is an important signature of PFis [15], [17].

B. CORRELATION ANALYSIS

The correlation between the proposed descriptors and the clinical PFis indices was investigated, with the Spearman correlation analysis showing that the statistical descriptors were negatively correlated with the BMI, the thickness and the VAS. That is, the lower the shear modulus (*mode, avg, med, qG*), the higher the clinical indices (BMI, thickness and VAS scores) tended to be. A strong correlation between Young's modulus and the clinical scores (FFI-pain, FFI-function, AOFAS) in symptomatic PFis has previously been shown by SWE imaging [24], which confirmed the findings of the present study. The texture descriptors also negatively correlated with the clinical indices. The lower the texture descriptor of shear modulus (*autoc, sosvh, savgh, and svarh*), the higher the clinical indices were likely to be.

The correlation analysis further confirmed the fact that softening (by statistical descriptors), and echotexture (by texture descriptors) of PF are signatures of PFis in the shear wave elastography. The VAS negatively correlated to both the statistical and texture descriptors, indicating that the proposed descriptors can reflect the degree of the PF pain.

C. ROC AND COFACTOR ROC ANALYSIS FOR THE DIAGNOSIS OF PLANTAR FASCIITIS

The PF thickness and the BMI were associated with PFis [3], [5], [9]–[11], [22], [36]. The ROC analysis of the clinical indices showed that the BMI and the thickness had AUCs $\leq$ 0.778(likelihood ratios $\leq$ 2.820). In contrast, ROC analyses showed that both the statistical descriptors (*mode, avg, med, qG*) and the texture descriptors (*autoc, sosvh, savgh, svarh*) were promising biomarkers, with AUCs of approximately 0.9 (likelihood ratio $\geq$ 6.798.) and 0.85 (likelihood ratio $\geq$ 3.195), respectively. The proposed statistical descriptors within the SROI can achieve higher AUCs (∼0.9) to identify PFis, which is superior to the results from previous work that used the mean value on multi-site PF regions (AUC ∼0.84) [24]. Our approach is also superior to other methods in which a radiologist used the color channel information over the entire PF for a qualitative assessment [14], [15], [17], [18]. The results indicate that the proposed descriptors are significant outcomes for PFis.

Furthermore, the Co Factors ROC analysis showed that the statistical descriptors performed better than the other parameters, as the features which only combined the statistical descriptors mostly achieved AUCs $\geq$ 0.93. The features that only combined the texture descriptors achieved AUCs of 0.86 $\sim$ 0.87. However, when only combining the clinical indices, the AUCs were $\leq$ 0.83. The diagnosis accuracy can be improved greatly when combining with the statistical descriptors or the texture descriptors, indicating that the statistical descriptors or the texture descriptors are favored for the diagnosis of PFis.

Most soft tissues such as breast, liver, lung and bone were reported to show different texture and statistical features between normal and diseased tissues [37], [38], extending the proposed descriptors to the diagnosis on other soft tissues are available. Additionally, the Co factors ROC analysis may be helpful to improve the diagnosis for many soft tissues.

D. THE PROTOCOL OF STANDARDIZED ROI

The PF was measured around the calcaneus attachment as this is the most frequently diseased site [2], [4], [21]. In this

TABLE 6. Twenty texture descriptors.

Variable	Formula	Annotation
autoc	$\sum_i \sum_j (ij)\, p(i,j)$	Autocorrelation
contr	$\sum_{n=0}^{G_n-1} n^2 \left\{ \sum_{i=1}^{G_n} \sum_{j=1}^{G_n} p(i,j) \, \|\|i-j\| = n \right\}$	Contrast
corrp	$\frac{\sum_i \sum_j (ij) p(i,j) - \mu_x \mu_y}{\sigma_x \sigma_y}$	Correlation
cprom	$\sum_i \sum_j (i + j - \mu_x - \mu_y)^4 p(i,j)$	Cluster prominence
cshad	$\sum_i \sum_j (i + j - \mu_x - \mu_y)^3 p(i,j)$	Cluster shade
dissi	$\sum_i \sum_j \|i-j\| \cdot p(i,j)$	Dissimilarity
energ	$\sum_i \sum_j p(i,j)^2$	Energy
entro	$-\sum_i \sum_j p(i,j) \log(p(i,j))$	Entropy
homop	$\sum_i \sum_j \frac{1}{1+(i-j)^2} p(i,j)$	Homogeneity
maxpr	$\max_{i,j} p(i,j)$	Maximum Probability
sosvh	$\sum_i \sum_j (i-\mu)^2 p(i,j)$	Sum of Squares: Variance
savgh	$\sum_{i=2}^{2G_n} i p_{x+y}(i)$	Sum Average
svarh	$\sum_{i=2}^{2G_n} \left(i - [-\sum_{i=2}^{2G_n} p_{x+y}(i) log\{p_{x+y}(i)\}] \right)^2 p_{x+y}(i)$	Sum Variance
senth	$-\sum_{i=2}^{2G_n} p_{x+y}(i) log\{p_{x+y}(i)\}$	Sum Entropy
dvarh	Variance of p_{x-y}	Difference Variance
denth	$-\sum_{i=0}^{G_n-1} p_{x-y}(i) \, log\{p_{x-y}(i)\}$	Difference Entropy
inf1h	$\frac{HXY - HXY1}{max\{HX, HY\}}$	Information Measures of Correlation1
inf2h	$(1 - \exp[-2.0(HXY2 - HXY)])^{1/2}$	Information Measures of Correlation2
indnc	$\sum_{i,j=1}^{G_n} \frac{p(i,j)}{1 + \|i-j\|/{G_n}^2}$	Inverse difference normalized
idmnc	$\sum_{i,j=1}^{G_n} \frac{p(i,j)}{1 + (i-j)^2/{G_n}^2}$	Inverse difference moment normalized

study, the statistical descriptors were measured on the SROI near the calcaneus attachment, as defined by the clinical ultrasound physician using the same protocol for every participant. The elliptic SROI was selected such that it reflected the PF elasticity but excluded adjacent non-relevant tissue. Following the same rules, the reproducibility of the measurement can be improved and valuable diagnostic criteria could be established. The results show that the statistical descriptors within the SROI can obtain clinical valuable biomarkers for diagnosing PFis.

It has been reported that not only the PF but also the surrounding tissues have elasticity changes in PFis [2], [21]. The texture descriptors can characterize the echovariation of the shear modulus of the PF and surrounding tissues, which were measured in the rectangular region including the PF, the fat pad and the calcaneus. The texture descriptors calculated from the GLCM are dependent of the interpixel distance (d) and orientation (θ). In this study, $d = 1$ and $\theta = 0, 90°$ were investigated. The texture descriptors from the horizontal and the vertical GLCM were in strong agreement. In both directions, the proposed texture descriptors are promising for the diagnosis of PFis.

V. CONCLUSIONS AND FUTURE WORK

In this study, the statistical descriptors of the shear modulus within SROIs and texture descriptors within the SWE measurement window were proposed to characterize the PF features. Our findings revealed that the distribution features of the shear modulus in the SROI (*mode, avg, med, qG*) and the image textures of shear modulus (*autoc, sosvh, savgh, svarh*) showed significant differences between the Healthy and the PFis groups. The statistical descriptors and the texture descriptors have AUCs of approximately 0.9 and 0.85 respectively, with high likelihood ratios. Combinations of statistical and texture descriptors can achieve higher AUCs ~0.968. These descriptors moderately correlated with the clinical indices (BMI and VAS) with Spearman coefficients $r = -0.5 \sim -0.4$. The proposed descriptors are potential imaging biomarkers which could be applied to clinical shear wave elastography for the diagnosis of PFis. The approach

described in this study may be extended to the elastography of other soft tissues.

Other populations, including patients with bilateral PFis will be included in future work. The texture descriptors were calculated only in one interpixel and two directions. The optimal interpixel and angle can be studied by testing additional combinations. The diagnosis of PFis by advanced machine learning methods will also be explored.

APPENDIX
TWENTY TEXTURE DESCRIPTORS FOR CHARACTERISTIC OF TEXTURE FEATURE

In this study, twenty texture descriptors were calculated from the GLCM. The following equations were used to define these texture features.

Let $p(i,j)$ denotes the (i,j)th entry in a normalized GLCM, and G_n the quantized number of grey levels. The mean and standard deviations for the rows and columns of the matrix are

$$\mu_x = \sum_i \sum_j i \cdot p(i,j), \quad \sigma_x = \sum_i \sum_j (i-\mu_x)^2 \cdot p(i,j),$$
$$\mu_y = \sum_i \sum_j j \cdot p(i,j), \quad \sigma_y = \sum_i \sum_j \left(j-\mu_y\right)^2 \cdot p(i,j).$$

Let $p_x(i) = \sum_{j=1}^{G_n} p(i,j)$ and $p_y(j) = \sum_{i=1}^{G_n} p(i,j)$ representing the ith entry in the marginal-probability matrix obtained by summing the rows and columns of $p(i,j)$ respectively.

The joint entropy is defined by $HXY = -\sum_i \sum_j p(i,j)\, log(p(i,j))$.

The entropy of p_x is $HX = -\sum_i \sum_j p_x(i) log(p(i,j))$.

The entropy of p_y is $HY = -\sum_i \sum_j p_y(j) log(p(i,j))$.

$$HXY1 = -\sum_i \sum_j p(i,j) log\left\{p_x(i)\, p_y(j)\right\}.$$
$$HXY2 = -\sum_i \sum_j p_x(i) p_y(j) log\left\{p_x(i)\, p_y(j)\right\}.$$
$$p_{x+y}(k) = \sum_{i=1}^{G_n} \sum_{j=1}^{G_n} p(i,j) | i+j = k, \quad k = 2, 3, \cdots, 2G_n.$$
$$p_{x-y}(k) = \sum_{i=1}^{G_n} \sum_{j=1}^{G_n} p(i,j) | |i-j| = k, \quad k = 2, 3, \cdots, 2G_n.$$

ACKNOWLEDGMENT

(Lei Xu is co-first author.)

REFERENCES

[1] S. K. Neufeld and R. Cerrato, "Plantar fasciitis: Evaluation and treatment," *J. Amer. Academy Orthopaedic Surgeons.*, vol. 16, no. 6, p. 338, 2008.

[2] S. C. Wearing, J. E. Smeathers, S. R. Urry, E. M. Hennig, and A. P. Hills, "The pathomechanics of plantar fasciitis," *Sports Med.*, vol. 36, no. 7, pp. 585–611, 2006.

[3] A. Radwan, M. Wyland, L. Applequist, E. Bolowsky, H. Klingensmith, and I. Virag, "Ultrasonography, an effective tool in diagnosing plantar fasciitis: A systematic review of diagnostic trials," *Int. J. Sports Phys. Therapy.*, vol. 11, no. 5, pp. 663–671, 2016.

[4] R. L. Martin, T. E. Davenport, S. F. Reischl, T. G. McPoil, J. W. Matheson, D. K. Wukich, C. M. McDonough, R. D. Altman, P. Beattie, M. Cornwall, and I. Davis, "Heel pain-plantar fasciitis: Revision 2014," *J Orthop Sports Phys Ther.*, vol. 44, no. 11, pp. A1–A33, 2014.

[5] F. Draghi, S. Gitto, C. Bortolotto, A. G. Draghi, and G. O. Belometti, "Imaging of plantar fascia disorders: Findings on plain radiography, ultrasound and magnetic resonance imaging," *Insights Imag.*, vol. 8, no. 1, pp. 69–78, Feb. 2017.

[6] M. Kim, Y. S. Choi, M.-W. You, J. S. Kim, and K. W. Young, "Sonoelastography in the evaluation of plantar fasciitis treatment: 3-Month follow-up after collagen injection," *Ultrasound Quart.*, vol. 32, no. 4, pp. 327–332, Dec. 2016.

[7] A. Mcmillan, K. Landorf, J. Barrett, H. Menz, and A. Bird, "Diagnostic imaging for chronic plantar heel pain: A systematic review and meta-analysis," *J. Foot Ankle Res.*, vol. 4, no. S1, p. 32, Dec. 2011.

[8] H. R. Osborne, W. H. Breidahl, and G. T. Allison, "Critical differences in lateral X-rays with and without a diagnosis of plantar fasciitis," *J. Sci. Med. Sport*, vol. 9, no. 3, pp. 231–237, Jun. 2006.

[9] H. P. Schneider, J. M. Baca, B. B. Carpenter, P. D. Dayton, A. E. Fleischer, and B. D. Sachs, "American college of foot and ankle surgeons clinical consensus statement: Diagnosis and treatment of adult acquired infracalcaneal heel pain," *J. Foot Ankle Surgery*, vol. 57, no. 2, pp. 370–381, Mar. 2018.

[10] E. Cardinal, R. K. Chhem, C. G. Beauregard, B. Aubin, and M. Pelletier, "Plantar fasciitis: Sonographic evaluation," *Radiology*, vol. 201, no. 1, pp. 257–259, 1996.

[11] F. J. Putz, M. G. Hautmann, M. C. Banas, and E. M. Jung, "Investigation of the acute plantar fasciitis with contrast-enhanced ultrasound and shear wave elastography—First results," *Clin. Hemorheology Microcirculat.*, vol. 67, nos. 3–4, pp. 415–423, Dec. 2017.

[12] T. L.-W. Chen, C. E. Agresta, D. B. Lipps, S. G. Provenzano, J. F. Hafer, D. W.-C. Wong, M. Zhang, and R. F. Zernicke, "Ultrasound elastographic assessment of plantar fascia in runners using rearfoot strike and forefoot strike," *J. Biomech.*, vol. 89, pp. 65–71, May 2019.

[13] M. S. Taljanovic, L. H. Gimber, G. W. Becker, L. D. Latt, A. S. Klauser, D. M. Melville, L. Gao, and R. S. Witte, "Shear-wave elastography: Basic physics and musculoskeltal applications," *Radiographics*, vol. 37, no. 3, pp. 855–870, 2017.

[14] C.-H. Wu, W.-S. Chen, and T.-G. Wang, "Plantar fascia softening in plantar fasciitis with normal B-mode sonography," *Skeletal Radiol.*, vol. 44, no. 11, pp. 1603–1607, Nov. 2015.

[15] L. M. Sconfienza, E. Silvestri, D. Orlandi, E. Fabbro, G. Ferrero, C. Martini, F. Sardanelli, and M. A. Cimmino, "Real-time sonoelastography of the plantar fascia: Comparison between patients with plantar fasciitis and healthy control subjects," *Radiology*, vol. 267, no. 1, pp. 195–200, Apr. 2013.

[16] S.-Y. Lee, H. J. Park, H. J. Kwag, H.-P. Hong, H.-W. Park, Y.-R. Lee, K. J. Yoon, and Y.-T. Lee, "Ultrasound elastography in the early diagnosis of plantar fasciitis," *Clin. Imag.*, vol. 38, no. 5, pp. 715–718, Sep. 2014.

[17] J. Ríos-Díaz, J. J. Martínez-Payá, M. E. del Baño-Aledo, A. de Groot-Ferrando, P. Botía-Castillo, and D. Fernández-Rodríguez, "Sonoelastography of plantar fascia: Reproducibility and pattern description in healthy subjects and symptomatic subjects," *Ultrasound Med. Biol.*, vol. 41, no. 10, pp. 2605–2613, Oct. 2015.

[18] C.-H. Wu, K.-V. Chang, S. Mio, W.-S. Chen, and T.-G. Wang, "Sonoelastography of the plantar fascia," *Radiology*, vol. 259, no. 2, pp. 502–507, May 2011.

[19] C.-Y. Lin, C.-C. Lin, Y.-C. Chou, P.-Y. Chen, and C.-L. Wang, "Heel pad stiffness in plantar heel pain by shear wave elastography," *Ultrasound Med. Biol.*, vol. 41, no. 11, pp. 2890–2898, Nov. 2015.

[20] K. Wang, J. Liu, J. Wu, Z. Qian, L. Ren, and L. Ren, "Noninvasive *in vivo* study of the morphology and mechanical properties of plantar fascia based on ultrasound," *IEEE Access*, vol. 7, pp. 53641–53649, 2019.

[21] H. Shiotani, R. Yamashita, T. Mizokuchi, M. Naito, and Y. Kawakami, "Site- and sex-differences in morphological and mechanical properties of the plantar fascia: A supersonic shear imaging study," *J. Biomech.*, vol. 85, pp. 198–203, Mar. 2019.

[22] S. Taş, N. Bek, M. Ruhi Onur, and F. Korkusuz, "Effects of body mass index on mechanical properties of the plantar fascia and heel pad in asymptomatic participants," *Foot Ankle Int.*, vol. 38, no. 7, pp. 779–784, Jul. 2017.

[23] L. Zhang, W. Wan, L. Zhang, H. Xiao, Y. Luo, X. Fei, Z. Zheng, and P. Tang, "Assessment of plantar fasciitis using shear wave elastography," *Nan Fang Yi Ke Da Xue Xue Bao= J. Southern Med. Univ.*, vol. 34, no. 2, pp. 206–209, Feb. 2014.

[24] M. Gatz, L. Bejder, V. Quack, S. Schrading, T. Dirrichs, M. Tingart, C. Kuhl, and M. Betsch, "Shear wave elastography (SWE) for the evaluation of patients with plantar fasciitis," *Academic Radiol.*, vol. 27, no. 3, pp. 363–370, Mar. 2020.
[25] L. M. Sconfienza, D. Orlandi, M. A. Cimmino, and E. Silvestri, "A few considerations on' sonoelastography of the plantar fascia,"' *Radiology*, vol. 261, no. 3, pp. 995–996, 2011.
[26] H. Zhang, M. Song, L. Ruan, F. Zhang, A. Zhang, A. M. Siedlecki, and M. Wan, "Von mises strain as a risk marker for vulnerability of carotid plaque: Preliminary clinical evaluation of cerebral infarction," *Ultrasound Med. Biol.*, vol. 45, no. 5, pp. 1221–1233, May 2019.
[27] S. R. Bowen, W. T. C. Yuh, D. S. Hippe, W. Wu, S. C. Partridge, S. Elias, G. Jia, Z. Huang, G. A. Sandison, D. Nelson, M. V. Knopp, S. S. Lo, P. E. Kinahan, and N. A. Mayr, "Tumor radiomic heterogeneity: Multiparametric functional imaging to characterize variability and predict response following cervical cancer radiation therapy," *J. Magn. Reson. Imag.*, vol. 47, no. 5, pp. 1388–1396, May 2018.
[28] C. Huang, Q. He, M. Huang, L. Huang, X. Zhao, C. Yuan, and J. Luo, "Non-invasive identification of vulnerable atherosclerotic plaques using texture analysis in ultrasound carotid elastography: An *in vivo* feasibility study validated by magnetic resonance imaging," *Ultrasound Med. Biol.*, vol. 43, no. 4, pp. 817–830, Apr. 2017.
[29] G.-M. Xian, "An identification method of malignant and benign liver tumors from ultrasonography based on GLCM texture features and fuzzy SVM," *Expert Syst. Appl.*, vol. 37, no. 10, pp. 6737–6741, Oct. 2010.
[30] K. Wang, X. Lu, H. Zhou, Y. Gao, J. Zheng, M. Tong, C. Wu, C. Liu, L. Huang, T. Jiang, F. Meng, Y. Lu, H. Ai, X.-Y. Xie, L.-P. Yin, P. Liang, J. Tian, and R. Zheng, "Deep learning radiomics of shear wave elastography significantly improved diagnostic performance for assessing liver fibrosis in chronic hepatitis B: A prospective multicentre study," *Gut*, vol. 68, no. 4, pp. 729–741, Apr. 2019. [Online]. Available:https://gut.bmj.com/content/68/4/729
[31] J. Gao, L. Xu, A. Bouakaz, and M. Wan, "A deep siamese-based plantar fasciitis classification method using shear wave elastography," *IEEE Access*, vol. 7, pp. 130999–131007, 2019.
[32] J. P. Jia, X. Q. He, and Y. J. Jin, "General measurement of data statistics," in *Statistics*, 6th ed., W. Wei, Ed. BeiJing, China: China Renmin Univ. Press, 2014, pp. 84–109.
[33] R. M. Haralick, K. Shanmugam, and I. H. Dinstein, "Textural features for image classification," *IEEE Trans. Syst., Man, Cybern.*, vol. SMC-3, no. 6, pp. 610–621, Nov. 1973.
[34] D. G. Barber and E. F. LeDrew, "SAR sea ice discrimination using texture statistics: A multivariate approach," *Photogramm. Eng. Remote Sens.*, vol. 57, no. 4, pp. 385–395, 1991.
[35] R.-E. Fan, P.-H. Chen, and C.-J. Lin, "Working set selection using second order information for training support vector machines," *J. Mach. Learn. Res.*, vol. 6, pp. 1889–1918, Dec. 2005.
[36] K. D. B. van Leeuwen, J. Rogers, T. Winzenberg, and M. van Middelkoop, "Higher body mass index is associated with plantar fasciopathy/'plantar fasciitis': Systematic review and meta-analysis of various clinical and imaging risk factors," *Brit. J. Sports Med.*, vol. 50, no. 16, pp. 972–981, Aug. 2016.
[37] B. Ganeshan, E. Panayiotou, K. Burnand, S. Dizdarevic, and K. Miles, "Tumour heterogeneity in non-small cell lung carcinoma assessed by CT texture analysis: A potential marker of survival," *Eur. Radiol.*, vol. 22, no. 4, pp. 796–802, Apr. 2012.
[38] T. Hodgdon, R. E. Thornhill, N. D. James, P. E. Beaulé, A. D. Speirs, and K. S. Rakhra, "CT texture analysis of acetabular subchondral bone can discriminate between normal and cam-positive hips," *Eur. Radiol.*, pp. 1–10, Apr. 2020, doi: 10.1007/s00330-020-06781-1.

HONGMEI ZHANG (Member, IEEE) received the Ph.D. degree in biomedical science and technology from Xi'an Jiaotong University, in 2004. She is currently an Associate Professor with the Key Laboratory of Biomedical Information Engineering, Ministry of Education, and with the Department of Biomedical Engineering, Xi'an Jiaotong University. Her multidisciplinary broad research interests include medical signal analysis, image analysis, and ultrasound viscoelastic imaging on early diagnosis and biomarkers for major disease. She has more than 20 publications as a first author. She is a member of the Chinese Institute of Electronics.

LEI XU received the bachelor's degree in medicine and the master's degree in imaging and nuclear medicine from Fourth Military Medical University. She is currently pursuing the Ph.D. degree with the Department of Biomedical Engineering, School of Life Science and Technology, Xi'an Jiaotong University. She is also a Radiologist with the Department of Medical Ultrasonic, Xi'an Hospital of Traditional Chinese Medicine. Her research interests include musculoskeletal ultrasound diagnosis, ultrasound elastography, and ultrasonic intervention treatment.

ZHIHUI LIU received the bachelor's degree in biomedical engineering from the University of Shanghai for Science and Technology, Shanghai, China, in 2018. She is currently pursuing the M.S. degree with the Department of Biomedical Engineering, School of Life Science and Technology, Xi'an Jiaotong University. Her research interests include ultrasound imaging, image processing, and viscoelastic imaging of carotid atherosclerotic plaque.

SHUKUAN LU (Associate Member, IEEE) was born in Shaanxi, China, in 1991. He received the B.S. and Ph.D. degrees from the Biomedical Engineering Department, Xi'an Jiaotong University, Xi'an, China, in 2013 and 2018, respectively.

He is currently a Postdoctoral Fellow with the Department of Biomedical Engineering, Xi'an Jiaotong University. His current research interests include ultrasound signal processing and beamforming, ultrasound passive cavitation mapping, and ultrasound therapy monitoring.

JICHAO YIN received the M.D. degree in orthopedics from the Shaanxi University of Traditional Chinese medicine, Xianyang, Shaanxi, in 2003.

He has been involved in the clinical research of osteoarthritis (musculoskeletal pain) for nearly 20 years. He is also an Associate Professor of orthopedics and a Master Tutor at the Shaanxi University of Traditional Chinese Medicine. His research interest includes the diagnosis and treatment of skeletal muscle pain by integrated traditional Chinese and western medicine. He is a Key Member of the Shaanxi Sanqin Scholar Innovation Team, participating in the national 973 project and 11 provincial and municipal scientific research projects. His awards and honors include the second prize of Provincial Science and Technology progress and the third prize of Municipal Science and Technology progress.

SIBO TIAN received the B.A. degree in biological sciences and economics from The University of Chicago, in 2009, and the M.D. degree from the Rutgers Robert Wood Johnson Medical School, New Brunswick, NJ, USA, in 2015. He is currently a Resident Physician in radiation oncology at the Winship Cancer Institute, Emory University, Atlanta, GA, USA. His research interests include the treatment of head and neck and thoracic malignancies, and the integration of ablative radiotherapy with immunotherapy. He was a recipient of the Conquer Cancer Merit Award at the 2018 ASCO Annual Meeting.

XIAOFENG YANG received the B.S., M.S., and Ph.D. degrees in biomedical engineering from Xi'an Jiaotong University, China. He finished his Ph.D. training and thesis at Emory University. He completed his postdoctoral and medical physics residency training at the Department of Radiation Oncology, Emory University School of Medicine, where he is currently an Assistant Professor of medical physics. His specialty is in image-guided intervention, deep learning multimodality medical imaging, and image registration and segmentation. He received many research awards, including the Best-in-Physics and Young Scientist Award from the American Association of Physicists in Medicine (AAPM) and SPIE Medical Imaging. He was a recipient of the John S. Laughlin Young Scientist Award of the AAPM.

MINGXI WAN (Member, IEEE) was born in Hubei, China, in 1962. He received the B.S. degree in geophysical prospecting from the Jianghan Petroleum Institute, Jingzhou, China, in 1982, and the M.S. and Ph.D. degrees in biomedical engineering from Xi'an Jiaotong University, Xi'an, China, in 1985 and 1989, respectively. From 1995 to 1996, he was a Visiting Professor with Drexel University, Philadelphia, PA, USA, and an Adjunct Professor with Pennsylvania State University, University Park, PA, USA. From 2001 to 2002, he was a Visiting Scholar with the Department of Biomedical Engineering, University of California at Davis, Davis, CA, USA. He has been a Professor and the Director of the Institute of Biomedical Engineering and Instrumentation, Xi'an Jiaotong University. He was the Chairman of the Department of Biomedical Engineering and the Dean of the School of Life Science and Technology, Xi'an Jiaotong University, from 1994 to 2006 and from 2000 to 2010, respectively. He has authored or coauthored more than 120 peer-reviewed publications in international journals and six books about medical ultrasound. His current research interests include ultrasonic imaging, especially in contrast and tissue perfusion evaluation, tissue elasticity imaging, therapeutic ultrasound, theranostics, and voice science. He received several important awards from the Chinese Government and university.